LA-UR-14-21431
Approved for public release; distribution is unlimited.

Title: Need for an (n, ) Apparatus at the LANSCE

Author(s): Koehler, Paul E.

Intended for: Description of potential new capability at LANSCE
Report

Issued: 2014-03-05

# Need for an ($n$,$\alpha$) Apparatus at the LANSCE

P. E. Koehler*
*LANSCE-NS*
(Dated: November 5, 2013)

There is an urgent need for a new ($n$,$\alpha$) measurement capability at the Los Alamos Neutrons Science Center (LANSCE) for several reasons. First, it has been shown that ($n$,$\alpha$) measurements on medium- to heavy-mass nuclides can provide some of the best constraints on some of the most important reaction rates for explosive nucleosynthesis studies. A few such measurements have been made, but many more are needed. Second, there are a few ($n$,$p$) and ($n$,$\alpha$) cross sections on lighter nuclides of importance to nuclear astrophysics that remain unmeasured. Third, it has been shown that ($n$,$\alpha$) measurements can constrain photon strength functions (PSFs) at very low energies. This is important because recent experiments, theory, and astrophysical calculations have demonstrated that enhanced PSFs at these energies can have large impacts on nucleosynthesis occurring in explosive environments. Also, enhanced low-energy PSFs could have significant impact on ($n$,$\gamma$) cross sections of interest to radiochemical diagnositics of nuclear devices. However, the shape of PSFs at low energies is a subject of considerable controversy, so new data are badly needed. Fourth, previous ($n$,$\alpha$) data have revealed a number of puzzles and hints of exotic atomic-nuclear interactions. In addition to being interesting in their own light, these interactions could be important for understanding high-energy-density environments such as in nuclear explosion and at the National Ignition Facility. Simulations indicate that the high neutron flux at the Manuel Lujan Jr. Neutron Scattering Center (MLNSC) at the LANSCE will make many more of the needed measurements feasible. Hence, a new ($n$,$\alpha$) instrument at the MLNSC would enable a wide range of important and interesting basic and applied science.

## I. INTRODUCTION

Although there have been relatively few ($n$,$p$) and ($n$,$\alpha$) measurements in the resolved- and unresolved-resonance ranges, much has been learned and many mysteries have been revealed. More detailed measurements on a wider range of samples hold the promise of having even greater impacts in a number of areas in basic and applied nuclear science. The main barriers to an expanded program are the small sizes of most of these cross sections, difficulties associated with producing the needed (in two cases) radioactive samples, and potentially large backgrounds. The neutron flux at the Manuel Lujan Jr. Neutron Scattering Center (MLNSC) at the Los Alamos Neutron Science Center (LANSCE) is much higher than that at all other facilities where previous ($n$,$p$) and ($n$,$\alpha$) measurements have been made. Hence, a much wider range of samples and expanded range of science should be accessible at MLNSC. As I show below, simulations indicate that the counting rates and time-of-flight resolution are sufficient to obtain the needed data. The main challenge appears to be reducing the $\gamma$-flash background at the beginning of each pulse to low enough levels. Techniques employed at other neutron sources should also work at MLNSC, although this remains to be demonstrated. In addition, a modern digital data acquisition system should make it possible for the first time to "compensate" (for the $\gamma$-flash) a gridded ion chamber, resulting in a large improvement in the data obtained.

*Electronic address: koehler@lanl.gov

There is a wide range of basic and applied nuclear science which could be addressed if this new capability was established. In the next section, I briefly describe some of these areas. Following this is a section describing counting-rate calculations for one subset of experiments. These calculations indicate experiments at MLNSC should be very worthwhile. The final two sections discuss expected challenging aspects of the proposed experiments and the overall outlook, respectively.

## II. MOTIVATION

The three interrelated fields of nuclear astrophysics, radiochemical diagnostics, and atomic-nuclear interactions are the main motivations for this new capability. In some cases, measurements will be aimed at obtaining a cross section or rate for a specific reaction of importance. In many cases the aim will be to improve theory across a global range so that the many cross sections beyond the reach of measurement can be estimated more accurately. Hence, a fourth overlapping motivation is testing and improving theory. Finally, the few experiments which have been done so far have revealed a number of surprises and led to different experiments and further surprises. In some cases, a single experiment has impacted several of the topics briefly described in the following subsections.

### A. Improving $\alpha-$nucleus reactions rates for explosive nucleosynthesis studies

The $p$ process is the name given to the mechanism through which neutron deficient isotopes of intermediate-

to heavy-mass elements are formed. In a leading model of the $p$ process, the shock front from type II supernova ignites explosive burning in oxygen/neon layers on a time scale of about 1 second and at temperatures between 2 and 3 billion degrees. Under these conditions, the $p$ nuclides are synthesized by photodisintegration reactions on $s$- and $r$-process seed nuclides (for more detail see Ref. [1]). The seed nuclides are shifted by $(\gamma,n)$ reactions to the point where $(\gamma,n)$ and $(n,\gamma)$ reactions are in equilibrium. Then, the reaction flow can proceed further only by $(\gamma,\alpha)$ and $(\gamma,p)$ reactions. Hence, $(\gamma,\alpha)$ reaction rates across a broad mass range play an important role in the extended network calculations that are required to describe the final $p$-process abundances [2].

However, there is at present no model of the $p$ process which can explain all the observed abundances, and many different astrophysical sites and scenarios have been proposed. Nevertheless, several studies (e.g., [3]) have confirmed that better rates for reactions involving $\alpha$ particles are needed for further progress.

Determination of $(\gamma,\alpha)$ rates at astrophysically relevant temperatures via direct measurements (or via inverse $(\alpha,\gamma)$ measurements) is exceedingly difficult because the corresponding energies are well below the Coulomb barrier so that the cross sections are extremely small. Therefore, very few measurements have been reported so far. In addition, very recently it has been shown [4] that Coulomb excitation is a significant effect in the $(\alpha,\gamma)$ channel and hence introduces additional uncertainty in the results.

In principle, the many needed rates should be calculable to sufficient accuracy using the nuclear statistical model (NSM). However, NSM calculations are hampered by the uncertain $\alpha$+nucleus optical potential in the astrophysically relevant energy range. The $\alpha$+nucleus optical potential is needed to calculate the transmission probability of the $\alpha$ particle through the Coulomb barrier of the nucleus and, therefore, has a large impact on the calculated rates. The potentials are thought to depend on several parameters related to the properties of the target nuclides, so it is important to have data across as wide a range of the parameter space as possible.

Typically, such potentials have been obtained by analysis of $\alpha$-elastic-scattering data. However, to reliably extract the potential, measurements must be made at energies significantly above the astrophysically interesting range. Therefore, it is necessary to extrapolate the results to lower energies, and it has been shown that such extrapolations introduce very large uncertainties.

In contrast, $Q$-values for $(n,\alpha)$ reactions correspond well with the astrophysically relevant range of the $p$ process, so extrapolations are not necessary. In addition, it has been shown [5, 6] that $(n,\alpha)$ cross sections are very sensitive to the $\alpha$ potential used in the statistical model. Also, scaling from previous measurements using predicted cross sections, indicates that $(n,\alpha)$ measurements for as many as 20 intermediate- to heavy-mass nuclides should be possible (see Section III). Hence, a series of $(n,\alpha)$ measurements may offer the best opportunity for enabling the needed global improvements in the $\alpha$+nucleus potential for astrophysics applications.

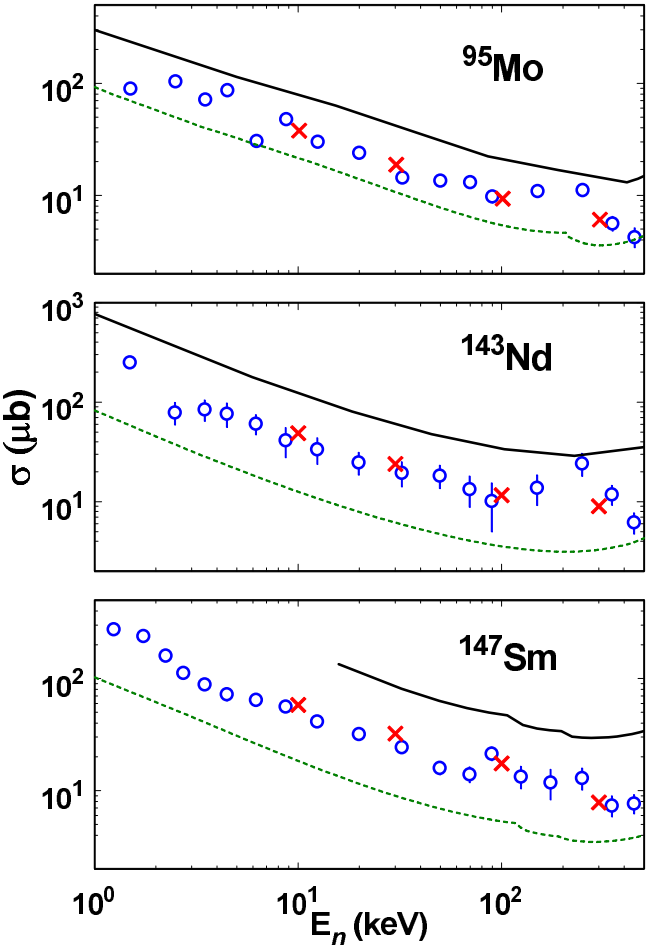


FIG. 1: $^{95}$Mo [7] (top), $^{143}$Nd [6], (middle), and $^{147}$Sm$(n,\alpha)$ [5] cross sections. Open blue circles depict measurements averaged over coarse energy bins. Cross sections calculated using three different NSM codes are shown as solid black curves [8], dashed red curves [9], and red X's [10].

For $p$-process nucleosynthesis studies, $(n,\alpha)$ cross-section measurements are needed in the mass range $A \approx 60-200$, across an energy range wide enough to allow useful comparison to NSM calculations. As shown in Fig. 1, for the three cases reported to date [5–7], $E_n \approx 1-10$ keV is sufficient. Shown in this figure are NSM calculations from three different codes using default parameters. The roughly factor of ten difference between cross sections predicted by the codes is typical, and is almost all due to the different $\alpha$-optical potentials employed. The challenge is to find a potential which has good predictive power across a wide mass range, and hence more data are needed to provide the needed constraints.

The previous measurements shown in Fig. 1 were all made at the Oak Ridge Electron Accelerator (ORELA) facility. The flux is orders of magnitude higher at MLNSC than at the ORELA. Hence, measurements on

a much wider range of samples should be possible at MLNSC, enabling the necessary global improvement in theory.

As explained in subsection II C, resonance analysis of the $(n,\alpha)$ data should result in even better constraints on the $\alpha$+nucleus potential. However, the few analyses of this type conducted so far have revealed that the situation is more complicated and more interesting than thought.

### B. Improving low-energy photon strength functions for astrophysics and radiochemical diagnostics

The presence of significant $^{143}$Nd(n,$\gamma\alpha$)$^{140}$Ce yield at thermal [11] and resonance [12] energies has been used to derive the $^{144}$Nd photon strength function (PSF) at low energies [13, 14]. The resulting PSF was relatively constant for photon energy between approximately 0.2 and 1.5 MeV, in conflict with the usual Lorentzian extrapolation of the giant dipole resonance, which falls to zero PSF at zero energy. This spurred the development of a new PSF theory [15] which was in much better agreement with these data.

More recent experiments, theory, and astrophysical calculations have demonstrated [16] that enhanced PSFs at low energies can have large impacts on nucleosynthesis occurring in explosive environments (e.g., during the $r$ process). Such and enhanced PSF also could have significant impact on $(n,\gamma)$ rates of interest to radiochemical diagnostics of nuclear devices because theory is used to predict most of these rates. However, the shape of PSFs at low energies is a subject of considerable controversy, so new data are badly needed.

In addition to the requirement of resolving several resonances, this application requires $\approx$ 300 keV $\alpha$-particle resolution; presence of $\alpha$ particles at energies between the discreet groups due to transitions to the ground and excited states of the residual nucleus being the signature of $(n,\gamma\alpha)$ reactions. In practice, this means reducing the sample thickness from that used in previous ORELA measurements. Hence, measurements for this application are even more demanding than for measuring average cross sections and average $\alpha$ widths. However, simulation results presented in Section III indicate that these measurements are feasible at the MLNSC.

### C. Non-statistical effects and problems with the $\alpha$+nucleus potential

As mentioned in subsection II A, even better constraints on the $\alpha$ potential can be obtained by comparing measured and theory average $\alpha$ widths $\langle\Gamma_\alpha\rangle$ rather than cross sections, thereby avoiding confounding uncertainties due to level-density and neutron parameters in the NSM. This approach requires resonance analysis of the $(n,\alpha)$ data, which in turn requires that the resonance spins, parities, neutron widths, and total radiation widths be known, or that data exist for determining these parameters. At present, sufficient published data exist for only $^{147}$Sm$(n,\alpha)^{144}$Nd, and the resulting analysis [17] indicates that the situation is more complicated and more interesting than thought.

Fig. 2 illustrates essential aspects of the $^{147}$Sm$(n,\alpha)^{144}$Nd reaction. Given the $^{147}$Sm ground-state spin and parity of $I^\pi = \frac{7^-}{2}$, $s$-wave resonances have $J^\pi = 3^-$ and $4^-$. However $4^-$ resonances are parity-forbidden from $\alpha$ decaying to the $0^+$ ground state of $^{144}$Nd. Given the large Coulomb barrier, it therefore is expected that the average $\alpha$ width $\langle\Gamma_\alpha\rangle$ for $4^-$ resonances will be substantially smaller than that for $3^-$ ones. Furthermore, given that the maximum resonance energy ($E_n \leq 700$ eV) analyzed was many orders of magnitude smaller than the relevant $\alpha$-particle energies, it was expected that the ratio of average $\alpha$ widths for the two $s$-wave spins would remain constant across the resonance-energy range analyzed. In contrast, it was found [17] that the $3^-$-to-$4^-$ $\langle\Gamma_\alpha\rangle$ ratio decreased rather dramatically near $E_n \approx 300$ eV. In subsequent analyses [18, 19] it was found that the reduced-neutron and total-radiation-width distributions, as well as the $^{147}$Sm$(n,\gamma)$ cross section also undergo significant changes near this energy. These observations are at present not understood. Therefore, it would be good to have similar data on nearby nuclides. For example, counting-rate estimates indicate that $^{149}$Sm$(n,\alpha)^{146}$Nd measurements should be feasible at the MLNSC. In addition, complementary $^{149}$Sm$(n,\gamma)$ data have already been taken with the Detector for Advanced Neutron Capture Experiments (DANCE), and reduced-neutron-width data exist from a previous total-cross-section measurement [20]. Hence, all the needed auxiliary data are already in hand for analyses similar to those reported for $^{147}$Sm.

Further examination of the $^{147}$Sm$(n,\alpha)$ data, as well as preliminary analysis of $^{95}$Mo and $^{143}$Nd$(n,\alpha)$ data reveals a common difference with respect to theory; measured $\langle\Gamma_\alpha\rangle$ values for non-natural-parity ($0^-$, $1^+$, $2^-$,...) resonances are much larger, relative to those for natural-parity resonances, than predicted by theory. This is illustrated for $^{95}$Mo in Fig. 3. This figure shows measured and theory $\langle\Gamma_\alpha\rangle$ ratios, relative to the $\langle\Gamma_\alpha\rangle$ for $2^+$ resonances. As can be seen, ratios predicted with the default $\alpha$ potential in the NSM TALYS [21] are in good agreement with the data for natural-parity resonances, but are substantially less than the data for non-natural-parity resonances. With the default $\alpha$ potential, TALYS overpredicts the $\langle\Gamma_\alpha\rangle$ values for natural-parity resonances by a factor of 6. When the $\alpha$ potential is adjusted to agree with the measured $\langle\Gamma_\alpha\rangle$ value for $2^+$ resonances, TALYS also is in good agreement with the measured $\langle\Gamma_\alpha\rangle$ values for the other two natural-parity resonances, but underpredicts $\langle\Gamma_\alpha\rangle$ for non-natural-parity resonances by an even larger amount than the default potential. Similar results are obtained with the other $\alpha$ potentials available in TALYS and for $^{143}$Nd and $^{147}$Sm.

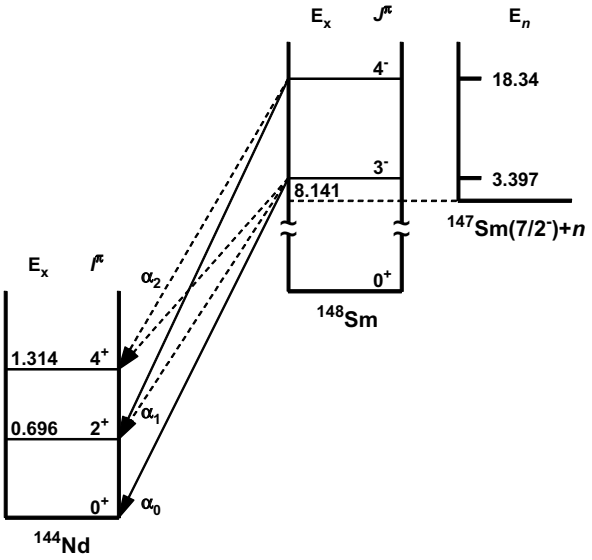


FIG. 2: Energy-level diagrams depicting the $^{147}$Sm$(n,\alpha)^{144}$Nd reaction ($Q$ = 10.127 MeV). Excitation (E$_x$) and laboratory neutron (E$_n$) energies are given in MeV and eV, respectively. Energy scales of the $^{144}$Nd and $^{148}$Sm parts of the figure differ by a factor of 17 million. $J^\pi = 3^-$ levels in $^{148}$Sm can $\alpha$ decay to the ground state of $^{144}$Nd, but $4^-$ ones are parity-forbidden from doing so. Both $3^-$ and $4^-$ levels in $^{148}$Sm can $\alpha$ decay to the first and second excited states of $^{144}$Nd, but with substantially reduced penetrability due to the large Coulumb barrier. As a result, it is expected that $\langle\Gamma_\alpha\rangle$ for $4^-$ resonances will be substantially smaller than that for $3^-$ ones.

In principle, measured $\langle\Gamma_\alpha\rangle$ values for non-natural-parity resonances could be enhanced significantly by the presence of substantial $(n,\gamma\alpha)$ cross section. The presence of $\alpha$-particle yield between the expected groups to the ground- and first-excited-state of $^{140}$Ce at thermal energy [11, 14] as well as for the 55- and 159-eV resonances [12] indicates that the $(n,\gamma\alpha)$ can make substantial contributions to the $\alpha$ yields for non-natural-parity resonances. In contrast, TALYS calculations predict that the average $(n,\gamma\alpha)$ cross section is negligible compared to the binary $(n,\alpha)$ cross section. Unfortunately, the relatively thick samples used in the ORELA experiments [17] resulted in such poor $\alpha$-particle resolution that it was not possible to distinguish $(n,\alpha)$ from $(n,\gamma\alpha)$. However, as discussed in Section III, the much higher flux at the MLNSC should allow the use of much thinner samples and hence make it possible to observe any significant $(n,\gamma\alpha)$ contributions to many more resonances.

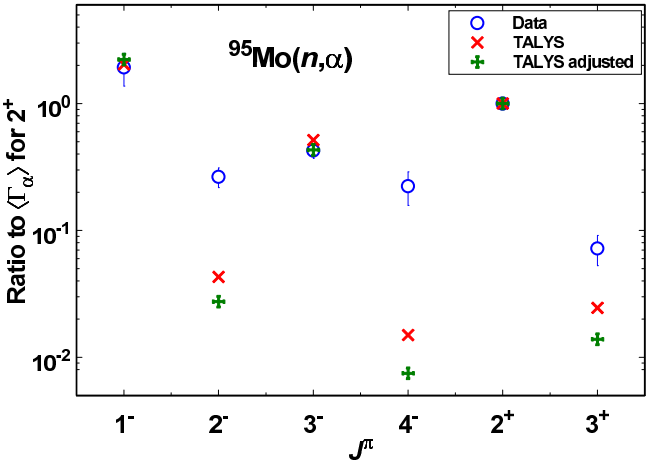


FIG. 3: Ratios of $\langle\Gamma_\alpha\rangle$ values from $^{95}$Mo$(n,\alpha)$ measurements and $\mathcal{R}$-matrix analysis, relative to the $\langle\Gamma_\alpha\rangle$ value for $2^+$ resonances. Results from experiment are shown as open blue circles with one-standard-deviation statistical error bars. Values predicted by TALYS with the default $\alpha$ potential are shown as red X's. Values predicted by TALYS, after the $\alpha$ potential was adjusted to yield agreement with the measured $\langle\Gamma_\alpha\rangle$ for $2^+$ resonances are shown as green crosses. Note that TALYS-predicted ratios for non-natural-parity resonances are substantially smaller than the data.

### D. Search for resonance internal conversion

An additional motivation for $(n,\alpha)$ measurements is more speculative but potentially very exciting: Abrupt changes in $^{147}$Sm neutron resonance parameters near $E_n = 300eV$ [17–19] as well as evidence of significant $^{143}$Nd$(n,\gamma\alpha)$ reactions [12] may be signs of atomic-nuclear interactions. In addition to being interesting in their own light, such interactions could be important for understanding of high-energy-density (HED) environments such as that in nuclear explosions and at the National Ignition Facility.

The experiment requirements are essentially the same as for the last two subsections; sufficient $\alpha$-particle resolution to resolve groups to the ground and first excited states of the residual nucleus. For example, the presence of an $\alpha_0$ group for a $4^-$ resonance in $^{143}$Nd [12] and substantially different $\alpha$ pulse-height spectra for different $3^-$ resonances in $^{147}$Sm have been interpreted as evidence for resonance internal conversion [22, 23] (RIC).

In RIC, the atomic electron remains bound rather than being ejected into the continuum as in ordinary internal conversion. The resonance character of this process can greatly amplify the ratio of the conversion width $\Gamma_c$ to the radiative width $\Gamma_\gamma$,

$$R = \frac{\Gamma_c}{\Gamma_\gamma} = \frac{2\alpha_d\Gamma}{\pi(4\Delta^2+\Gamma^2)}, \quad (1)$$

where $\alpha_d$ is a resonance analog for the usual coefficient of internal conversion coefficient, $\Delta$ is the resonance defect,

equal to the difference between the energies of the atomic and nuclear levels ($\Delta = E_a - E_n$), and $\Gamma$ is the total width of the resonance, equal to the sum of the atomic and nuclear widths. The maximum in $R$ occurs when the atomic and nuclear energies are equal; the probability of which is greatly enhanced by the high nuclear level density near the neutron threshold. Hence, the neutron-resonance region appears to be an excellent place in which to search for signatures of RIC. For example, a $4^-$ neutron resonance in $^{147}$Sm could transition via RIC to a nearby $3^-$, $4^+$, or $5^-$ level which could then $\alpha$ decay (because it is no longer parity forbidden) to the ground state of $^{144}$Nd; hence, an $\alpha_0$ group for a non-natural-parity resonance can be interpreted as a signature of RIC.

The probability of a neutron resonance decaying via RIC is given by,

$$W = (1 + R)\frac{\Gamma_i}{\Gamma_0}, \tag{2}$$

where $\Gamma_i$ is the partial width for the transition and $\Gamma_0$ the total width of the neutron resonance. Unfortunately, next to nothing is known about PSFs (and hence $\Gamma_i$) at very low energies (<100 keV). Assuming a constant PSF down to the lowest energies, as suggested by extrapolation of the above-mentioned results for $^{144}$Nd, would result in a probability which decreases as $E_\gamma^3$ for dipole radiation. Estimates based on this assumption, together with calculated $\alpha_d$ values and relevant widths for Sm atomic transitions of 1.6, 2.8, 46830, and 46832 eV indicate that $W \sim 10^{-7}$ to $10^{-2}$ [22], which appears to be too small to account for the above-mentioned effects in the $^{143}$Nd and $^{147}$Sm($n$,$\alpha$) reactions. However, recent measurements (e.g. [24–26]) as well as calculations [27, 28] indicate that PSFs increase significantly with decreasing energy in many nuclides, including $^{96}$Mo and $^{144}$Nd. Also, pronounced deviations from the mean values as well as non-statistical effects are possible for individual resonances. Therefore, the probability of RIC may be substantially higher than calculated in Ref. [22]. There also are many more possible atomic transitions than the few for which calculations were done in Ref. [22]. In particular, there are several possible transitions in Sm with energies near 350 eV, which is very close to the neutron resonance energy where the strange effects were observed in $\alpha$ [17], neutron [18], and $\gamma$ [19] widths for $^{147}$Sm neutron resonances.

Finally, RIC is the inverse of NEET (nuclear excitation by electron transition), which is the subject of an experimental search [29] because of its potential importance in HED environments.

## III. COUNTING-RATE ESTIMATE

Proposed experiments fall into two categories. First, experiments to measure average ($n$,$\alpha$) cross sections of importance to explosive nucleosynthesis (subsection II A) require only modest time-of-flight and $\alpha$-energy resolution and so can be done on a relatively short flight path with comparatively thick samples, thus allowing the widest range of samples to be measured. A schematic diagram of the ($n$,$\alpha$) apparatus used [5–7, 17] for several measurements of this type at the ORELA is shown in Fig. 4. The neutron beam was collimated to 10 cm diameter and the minimum normal flight path length (8.8 m) at the ORELA was used to obtain maximum flux. A 0.76-mm thick Cd filter was used to eliminate overlap slow neutrons from previous pulses and a 1.27-cm thick Pb filter was used to help reduce overload effects from the $\gamma$ flash at the start of each neutron pulse. Two samples (typically 11 cm diameter by ∼5 mg/cm$^2$ thick) were placed back to back in the center of a parallel-plate compensated ionization chamber (CIC) [30].

Calculated sample sizes needed for this apparatus are given in Table I. This table also contains a few lighter nuclides of interest to nuclear astrophysics for which ($n$,$\alpha$) and/or ($n$,$p$) measurements should be possible. Sample sizes were scaled to $^{17}$O($n$,$\alpha$) measurements at the ORELA [30] using NSM-predicted [31] average cross sections at 30 keV. The same or similar apparatus could be used at the MLNSC. Assuming a flight path length of 10 m, the flux at the MLNSC is at least 100 times larger than that used at the ORELA over the relevant energy range. Therefore, estimated sample sizes for Lujan-Center experiments are at least 100 times smaller than those given in column 5 of this table. Of the 30 nuclides listed in this table, 3 have been measured at the ORELA and used to test and improve the $\alpha$-potential for astrophysics applications; $^{95}$Mo [7], $^{143}$Nd [6], and $^{147}$Sm [5]. Assuming the NSM-predicted cross sections are reasonably accurate, average ($n$,$\alpha$) cross sections for most of the remaining nuclides in Table I should be measurable at the MLNSC.

Several of the nuclides in Table I are good candidates for studying low-energy PSFs and ($n$,$\gamma\alpha$) reactions, and searching for RIC as discussed above. However, better $\alpha$ pulse-height and time-of-flight resolution are needed for these applications. To these ends, gridded, multi-section ionization chambers, such as those shown in Fig. 5 [32] could be used. The grids and thinner samples (0.2 to 0.45 mg/cm$^2$) result in much better $\alpha$ pulse-height resolution, but at the expense of a more limited neutron energy range due to $\gamma$-flash effects and lower counting rate per sample area. With the electronics used in previous measurements, it was not possible to compensate a gridded chamber. However, as I explain in the next section, using a transient-digitizer-based data acquisition system should solve this problem, allowing good $\alpha$ pulse-height resolution measurements to be made to much higher neutron energies.

The flux is much higher and the pulse width 8 times narrower at the MLNSC than at the IBR facility at the Joint Institute for Neutron Research (JINR) in Dubna, Russia where previous measurements of this type were

TABLE I: Possible $(n,\alpha)$ measurement candidates

| Reaction | $Q$-value (MeV) | $\langle\sigma\rangle_{30}$ ($\mu$b)[a] | % Abundance | $m_{calc}$ (g)[b] |
|---|---|---|---|---|
| $^{32}$S($n$,$\alpha$)$^{29}$Si | 1.525 | 8.7 | 95.02 | 0.036 |
| $^{36}$Ar($n$,$\alpha$)$^{33}$S | 2.001 | 49 | 0.337 | 0.0072 |
| $^{43}$Ca($n$,$\alpha$)$^{40}$Ar | 2.286 | 1.4 | 0.135 | 0.30 |
| $^{45}$Sc($n$,$p$)$^{45}$Ca | 0.526 | 9.1 | 100 | 0.048 |
| $^{44}$Ti($n$,$p$)$^{44}$Sc | 1.049 | 16000 | 47.3 yr | $3.0\times10^{-6}$ |
| $^{44}$Ti($n$,$\alpha$)$^{41}$Ca | 3.235 | 560 | 47.3 yr | $7.8\times10^{-4}$ |
| $^{50}$V($n$,$p$)$^{50}$Ti | 2.999 | 390 | 0.25 | 0.0013 |
| $^{59}$Ni($n$,$\alpha$)$^{56}$Fe | 5.093 | 6400 | $7.5\times10^{4}$ yr | $90\times10^{-9}$ |
| $^{61}$Ni($n$,$\alpha$)$^{58}$Fe | 3.574 | 3.5 | 1.13 | 1.7 |
| $^{64}$Zn($n$,$\alpha$)$^{61}$Ni | 3.866 | 240 | 48.6 | 0.026 |
| $^{67}$Zn($n$,$\alpha$)$^{64}$Ni | 4.879 | 310 | 4.1 | 0.0021 |
| $^{73}$Ge($n$,$\alpha$)$^{70}$Zn | 3.913 | 0.11 | 7.8 | 6.5 |
| $^{77}$Se($n$,$\alpha$)$^{74}$Ge | 4.467 | 2.8 | 7.6 | 0.27 |
| $^{91}$Zr($n$,$\alpha$)$^{88}$Sr | 5.660 | 3.7 | 11.32 | 0.24 |
| $^{94}$Mo($n$,$\alpha$)$^{91}$Zr | 5.129 | 0.18 | 9.25 | 5.2 |
| $^{95}$Mo($n$,$\alpha$)$^{92}$Zr | 6.389 | 19 | 15.92 | 0.05 |
| $^{97}$Mo($n$,$\alpha$)$^{94}$Zr | 5.368 | 0.15 | 9.55 | 6.4 |
| $^{96}$Ru($n$,$\alpha$)$^{93}$Mo | 6.381 | 15 | 5.52 | 0.06 |
| $^{99}$Ru($n$,$\alpha$)$^{96}$Mo | 6.822 | 43 | 12.7 | 0.02 |
| $^{101}$Ru($n$,$\alpha$)$^{98}$Mo | 5.801 | 0.21 | 17.0 | 4.7 |
| $^{105}$Pd($n$,$\alpha$)$^{102}$Ru | 6.333 | 0.73 | 23.33 | 1.4 |
| $^{106}$Cd($n$,$\alpha$)$^{103}$Pd | 5.979 | 0.12 | 1.25 | 8.7 |
| $^{120}$Te($n$,$\alpha$)$^{117}$Sn | 6.636 | 0.25 | 0.096 | 4.7 |
| $^{123}$Te($n$,$\alpha$)$^{120}$Sn | 7.578 | 2.9 | 0.908 | 0.42 |
| $^{143}$Nd($n$,$\alpha$)$^{140}$Ce | 9.718 | 24 | 12.18 | 0.06 |
| $^{145}$Nd($n$,$\alpha$)$^{142}$Ce | 8.729 | 1.1 | 8.30 | 1.3 |
| $^{147}$Sm($n$,$\alpha$)$^{144}$Nd | 10.114 | 32 | 15.0 | 0.04 |
| $^{149}$Sm($n$,$\alpha$)$^{146}$Nd | 9.426 | 3.2 | 13.8 | 0.45 |
| $^{171}$Yb($n$,$\alpha$)$^{168}$Er | 9.327 | 0.10 | 14.3 | 16.9 |
| $^{177}$Hf($n$,$\alpha$)$^{174}$Yb | 9.711 | 0.12 | 18.6 | 14.6 |

[a] Refs. [10, 31].
[b] Amount of sample material needed for measurements at ORELA. Calculated by scaling to measurements of Ref. [30].

made. So it should be possible to study the science described above much better. Counting rates at the MLNSC were calculated using the measured flux [33] on flight path 4, scaled to a flight-path length of 60 m used in the simulation and a proton current of 100 $\mu$A. Channel widths were calculated to be equal to one half the resolution width assuming a pulse width from the proton storage ring of 125 ns and a moderation time spread in $\mu$s equal to $\Delta t_m = 1.5/\sqrt{E}$, for neutron energy $E$ in eV. I assumed the detector efficiency was 50%; all $\alpha$ particles emitted into each section of the chamber were detected. Statistical fluctuations in the counting rates were calculated by sampling from normal distributions with standard deviations equal to the square root of the average counting rate for each channel.

The $\mathcal{R}$-matrix code SAMMY [34] was used to calculate $^{143}$Nd and $^{151}$Sm($n$,$\alpha$) cross section from resonance parameters determined at the ORELA, using the MLNSC source resolution function determined with the Detector for Advanced Neutron Capture Experiments (DANCE). These cross sections together with a sample thickness of 0.2 mg/cm$^2$ (of $Nd_2O_3$ or $Sm_2O_3$) and area of 0.6 m$^2$ (the same parameters as the thinner samples used in Ref. [32]) and experiment parameters given in the preceding paragraph were used to calculate counting rates shown in Figs. 6 and 7.

Although parameters for the simulations shown in these two figures are among the most demanding anticipated, the counting-rate estimates are very encouraging. They indicate that $\alpha$ pulse-height spectra can be obtained for about 10 resonances of each spin for each of the two nuclides. This would be a large improvement over previous experiments and so should make possible a much better study of PSFs at low $\gamma$-ray energy and high

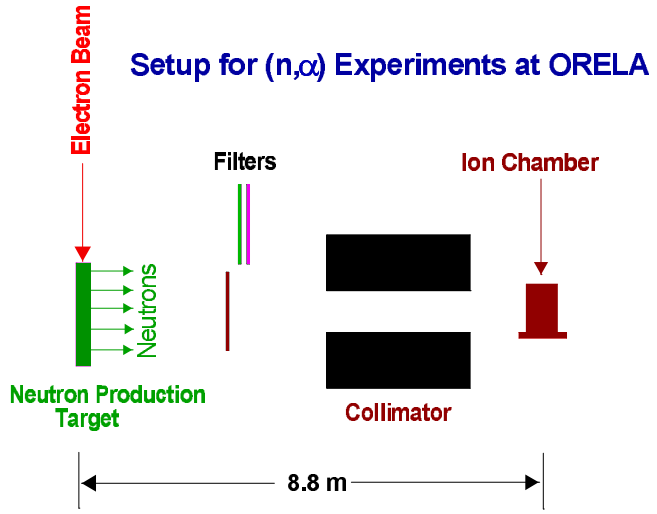


FIG. 4: Schematic (not to scale) diagram of the $(n,\alpha)$ apparatus at the ORELA. A 150-MeV pulsed electron beam from the accelerator impinged on a water-cooled tantalum neutron-production target. A collimator defined a 10-cm diameter neutron beam at the center of the detector. Cd and Pb filters were placed in the beam to eliminate wrap-around neutrons and reduce $\gamma$-flash effects, respectively.

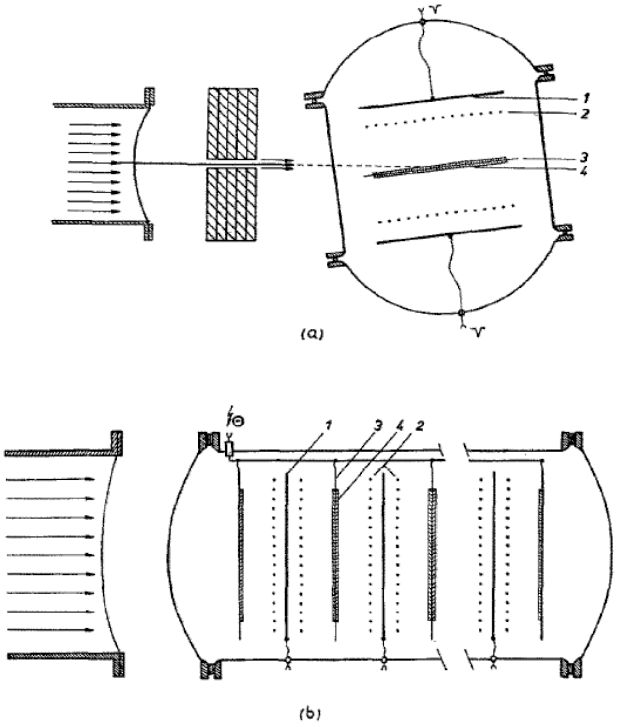


FIG. 5: Schematic diagrams of two different gridded ionization chambers used [32] for $(n,\alpha)$ measurements at the IBR pulsed reactor at the Joint Institute for Neutron Research in Dubna, Russia. The apparatus shown in (a) was used with a flight-path length of 30 m. It was designed to minimize $\gamma$-flash effects; hence, the samples are tilted with respect the beam direction and a collimator limits the volume of gas exposed to the beam. A larger sample can be accomodated in the apparatus shown in (b), at the expense of a reduced neutron energy range due to larger $\gamma$-flash effects. It was used with a flight-path length of 100 m. Collectors are labeled 1, grids 2, high voltage electrodes 3, and samples 4.

excitation as well as a better search for evidence of RIC and perhaps unequivocal evidence for this exotic phenomenon. Because they have similar cross sections and average level spacings, such measurements also should be possible on $^{95}$Mo and $^{99}$Ru. These nuclides are of particular interest because a sharp upbend in the PSF at low energies has been reported [24, 25]. Although the upbend has been challenged [35], its existence is supported by recent complementary measurements [26]. Similar $(n,\gamma\alpha)$ measurements also may be possible for $^{123}$Te and $^{149}$Sm. Although the cross sections are about 10 times smaller for these two cases, their smaller average resonance spacing should make it possible to measure $\alpha$ pulse-height spectra for very low energy resonances where both the flux and cross section are highest.

## IV. CHALLENGES

The main challenge appears to be overcoming effects due to the $\gamma$ flash at the start of each neutron pulse. Although each $\gamma$ ray does not cause much ionization, there are so many of them all arriving at the same time at the start of each pulse that together they cause a large overload signal in conventional preamplifiers and amplifiers. The time it takes the system to recover from this overload can severly limit the upper neutron energy range of the experiment. The number of neutrons per proton is much larger at the MLNSC than the number of neutrons per electron at the ORELA and IBR facilities. This should help to lessen $\gamma$-flash effects at the MLNSC compared to the other two facilities where previous $(n,\alpha)$ measurements were made. On the other hand, the duty factor is much lower (20 vs. 525 Hz) and average current higher (100 vs. 50 $\mu$A) at the MLNSC than the ORELA, both of which will worsen $\gamma$-flash effects.

Average $(n,\alpha)$ cross-section measurements for improving the $\alpha$ potential will need to be made to at least $E_n = 10$ keV. Because only the total $(n,\alpha)$ cross section is needed, this application does not require good $\alpha$ pulse-height resolution, and so relatively thick samples and a non-gridded ion chamber can be used. Therefore, a parallel-plate CIC such as that used in previous measurements at the ORELA [5–7, 30] likely will be sufficient. For the anticipated flight path length of 10 m, the detection system will need to recover from the $\gamma$ flash in less than 7.2 $\mu$s. Given that measurements with a relatively large CIC have been made to energies as high as several hundred keV at the ORELA with a flight path length of 8.8 m, it seems reasonable to assume that the necessary performance can be achieved at the MLNSC. The principle of operation of a CIC is illustrated in Fig.

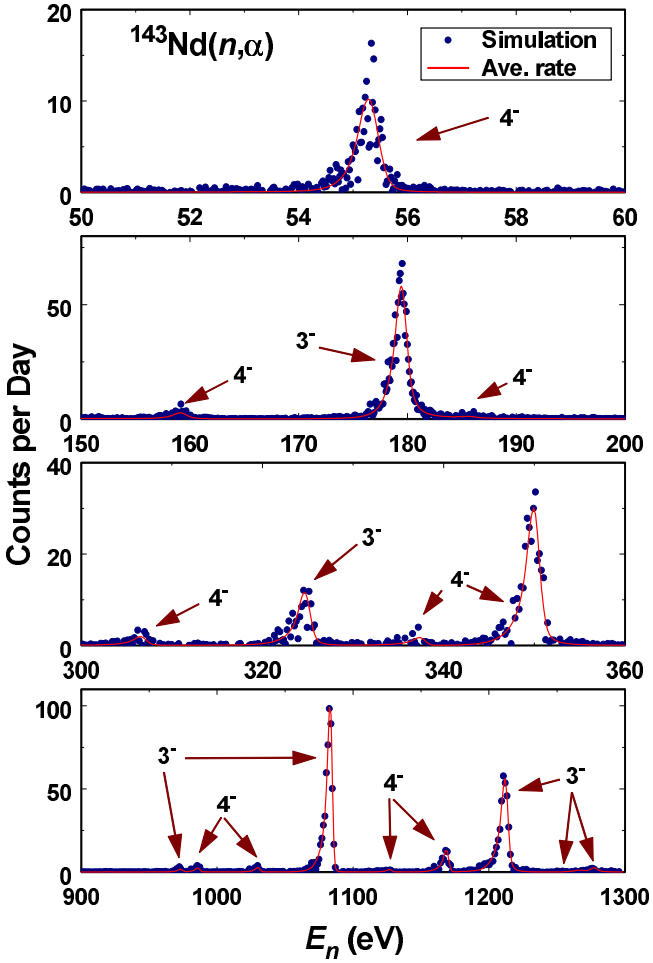


FIG. 6: Simulated counting rate for $^{143}$Nd(n,$\alpha$) experiment at the MLNSC for four representative regions. A flight path length of 60 m, and a sample ($Nd_2O_3$) thickness of 0.2 mg/cm$^2$ and area of 0.6 m$^2$ were assumed. The red curve is the calculated average counting rate per day per channel and the blue circles are simulated rates including counting statistics. Resonances are labeled with their $J^\pi$ assignments. See text for details.

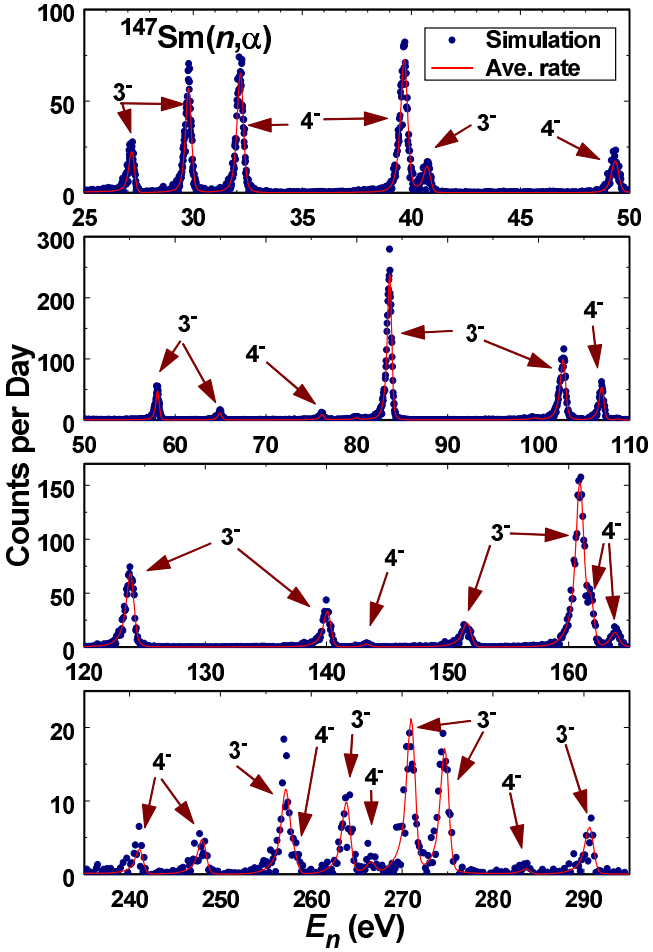


FIG. 7: Simulated counting rate for $^{147}$Sm(n,$\alpha$) experiment at the MLNSC for four representative regions. The red curve is the calculated average counting rate per day per channel and the blue circles are simulated rates including counting statistics. Resonances are labeled with their $J^\pi$ assignments. See text and caption of Fig. 6 for details.

8.

Experiments to constrain low-energy PSFs via ($n$,$\gamma\alpha$) measurements and to search for RIC need ~300 keV or better $\alpha$ pulse-height resolution and so require thinner samples and a gridded ion chamber (GIC). It also will be necessary to resolve as many resonances as possible, so a longer flight path length is needed. In the simulations above, I assumed a flight path length of 60 m as a good compromise between flux and resolution and because the silo on flight path 5 is at this distance from the neutron source. Also, given the relativly long proton pulse width from the proton storage ring, it is unlikely that any useful resonance information can be obtained above about 2 keV. The longer flight-path length and lower maximum energy lengthen the $\gamma$-flash recovery time to almost 100 $\mu$s. If the GIC cannot be made to recover satisfactorily in this time, it may be possible to compensate it and hence obtain quicker recovery in the following way. Refering to part b of Fig. 5, the signal from the first collector could be inverted and fanned in with the signal from the second collector. In this way, signals induced by ionization from the $\gamma$ flash in the first two sections of the detector (a section being defined as the volume between a high-voltage electrode and a collector) would cancel that due to the $\gamma$ flash in the next two sections. On the other hand signals due to $\alpha$ particles in the first two sections would be opposite polarity, but at different times (except for rare random coincidences) from signals due to $\alpha$ particles in the second two sections. Such an approach was not attempted in the past because typical amplifier and ADC systems could not handle signals of both polarities. However, this should be possible with modern transient-digitizer-based data-aquistion systems.

Obtaining the relatively large total sample areas needed for this latter class of experiments will likely require a GIC with on the order of 30 samples. While

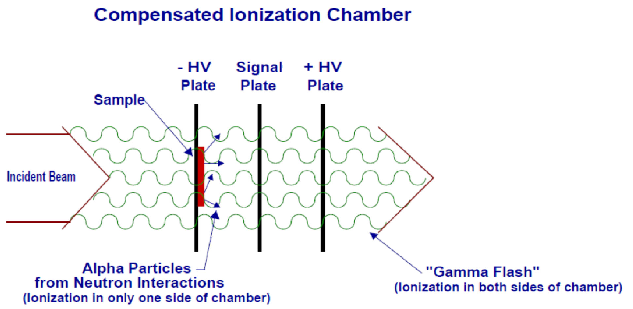


FIG. 8: Schematic diagram showing the principle of operation of a pulse-mode parallel-plate compensated ion chamber (CIC). In an ordinary parallel-plate ion chamber, the sample is placed on a plate held at negative high voltage and the signal is taken from the parallel plate at ground potential. Alpha particles from $(n,\alpha)$ reactions in the sample ionize the gas between the two plates, inducing a signal in a charge-sensitive preamplifier connected to the signal plate. The $\gamma$ flash at the start of each neutron pulse causes so much ionization in the gas that the preamplifier is overloaded. A CIC solves this problem by the addition of another plate at equal but opposite high voltage, on the opposite side of the signal plate as the original high voltage plate, with the same inter-plate distance. Now, when the $\gamma$ flash transits the CIC it induces equal (within statistics) but opposite signals on the central plate, thereby greatly reducing $\gamma$-flash effects.

this represents a challenge, such detectors have been constructed and operated in the past. This task should be much easier with modern electronics and data acquisition systems, for which 30 channels is a fairly small number.

There might be an alternative to using a GIC. Glass scintillators routinely have been used at the ORELA as neutron flux monitors and neutron detectors for total-cross-section measurements. For this application, the glass was loaded with 6.6% Li enriched to 95% in $^6$Li. Their fast response and relatively low sensitivity to $\gamma$ rays made these scintillators ideal for these applications. It might be possible to obtain similar scintillators loaded with the $(n,\alpha)$ sample of choice instead of $^6$Li. Alternatively, a thin coating of the sample might be placed on a $^6$Li-free glass scintillator or between two layers of scintillator. A stack of these "sandwhiches" might be used to obtain the needed sample size. The scintillators would be viewed edge on as was the typical practice at the ORELA. If this detector could be made to work, it would be more compact and have faster time response than a GIC.

## V. OUTLOOK

The interrelated fields of nuclear astrophysics, radiochemical diagnostics, atomic-nuclear interactions, and testing and improving nuclear theory all could benefit from a new $(n,\alpha)$ measurement capability at the MLNSC. Counting-rate estimates indicate that the large flux at the MLNSC will enable a much wider and detailed range of measurements than previously possible. In addition to the usual basic- and applied-science sponsors of nuclear-physics research at LANSCE, these experiments also are of potential interest to those trying to understand the science of HED environments.


[1] M. Rayet, N. Prantzos, and M. Arnould, Astron. Astrophys. **227**, 271 (1990).
[2] M. Rayet *et al.*, Astron. Astrophys. **298**, 517 (1995).
[3] T. Rauscher, Phys. Rev. C **73**, 015804 (2006).
[4] T. Rauscher, Phys. Rev. Lett. **111**, 061104 (2013).
[5] Y. M. Gledenov *et al.*, Phys. Rev. C **62**, 042801(R) (2000).
[6] P. E. Koehler *et al.*, Nucl. Phys. **A688**, 86c (2001).
[7] W. Rapp, P. E. Koehler, F. Käppeler, and S. Raman, Phys. Rev. C **68**, 015802 (2003).
[8] T. Rauscher and F. K. Thielemann, Atomic Data Nucl. Data Tables **75**, 1 (2000), http://nucastro.org/nonsmoker.html.
[9] S. Goriely, in *Nuclei in the Cosmos*, edited by N. Prantzos and S. Harissopulos (Editions Frontieres, Paris, 1998), p. 314.
[10] J. A. Holmes, S. E. Woosley, W. A. Fowler, and B. A. Zimmerman, At. Data Nucl. Data Tables **18**, 305 (1976).
[11] L. Aldea and H. Seyfarth, in *Proceedings of the Third International Symposium on Neutron Capture Gamma-Ray Spectroscopy and Related Topics*, edited by R. E. Chrien and W. R. Kane (Plenum Press, New York, 1979), p. 526.
[12] J. Andrejewski, V. K. Thanh, V. Vtiurin, and Y. Popov, Technical Report No. P3-81-433, Joint Institute for Neutron Research (unpublished).
[13] V. Vtiurin and Y. Popov, Technical Report No. P3-82-309, Joint Institute for Neutron Research (unpublished).
[14] Y. P. Popov, in *Proceedings of the Europhysics Topical Conference*, edited by P. Oblozinsky (Institute of Physics, Bratislava, Smolenice, 1982), Vol. 10, p. 121.
[15] S. Kadmensky, V. Markushev, and W. Furman, Technical Report No. P4-82-210, Joint Institute for Neutron Research (unpublished).
[16] A. C. Larsen and S. Goriely, Phys. Rev. C **82**, 014318 (2010).
[17] P. E. Koehler, Y. M. Gledenov, T. Rauscher, and C. Frōhlich, Phys. Rev. C **69**, 015803 (2004).
[18] P. E. Koehler *et al.*, Phys. Rev. C **76**, 025804 (2007).
[19] P. E. Koehler *et al.*, Phys. Rev. Lett. **108**, 142502 (2012).
[20] M. Mizumoto, Nucl. Phys. **A357**, 90 (1981).
[21] A. J. Koning, S. Hilaire, and M. C. Duijvestijn, in *Proceedings of the International Conference on Nuclear Data for Science and Technology - ND2007*, edited by O. Bersillon *et al.* (EDP Sciences, Les Ulis, France, 2008), p. 211.
[22] Y. P. Gangrskii *et al.*, PisŠma v Zhurnal Fizika Elementarnykh Chastits i Atomnogo Yadra **6**, 90 (2006).

[23] Y. P. Gangrskii *et al.*, Physics of Particles and Nuclei Letters **3**, 395 (2006).
[24] M. Guttormsen *et al.*, Phys. Rev. C **71**, 044307 (2005).
[25] M. Guttormsen *et al.*, arXiv:0801.4667v1, 2008.
[26] M. Wiedeking *et al.*, Phys. Rev. Lett. **108**, 162503 (2012).
[27] I. Daoutidis and S. Goriely, Phys. Rev. C **86**, 034328 (2012).
[28] E. Litvinova and N. Belov, Phys. Rev. C **88**, 031302 (2013).
[29] P. Chodash *et al.*, in *Bulletin of the American Physical Society* (American Physical Society, New York, 2013), No. 13.
[30] P. E. Koehler, J. A. Harvey, and N. W. Hill, Nucl. Instr. and Meth. **A361**, 270 (1995).
[31] S. E. Woosley, W. A. Fowler, J. A. Holmes, and B. A. Zimmerman, At. Data Nucl. Data Tables **22**, 371 (1978).
[32] Y. P. Popov *et al.*, Nucl. Phys. **A188**, 212 (1972).
[33] P. E. Koehler, Nucl. Instr. and Meth. **A292**, 541 (1990).
[34] N. M. Larson, Technical Report No. ORNL/TM-9179/R8, Oak Ridge National Laboratory (unpublished).
[35] S. A. Sheets *et al.*, Phys. Rev. C **79**, 024301 (2009).